Original Manuscript

Title: Electrical Fields Induced Inside the Rat Brain with Skin, Skull, and Dural Placements of the Current Injection Electrode

Ahmet S. Asan, MS
Department of Biomedical Engineering
New Jersey Institute of Technology
University Heights
Newark, NJ 07102 USA

Sinan Gok, PhD
Department of Biomedical Engineering
New Jersey Institute of Technology
University Heights
Newark, NJ 07102 USA

Mesut Sahin, PhD
Professor of Biomedical Engineering
Associate Editor, IEEEE Tran. on Biomedical Circuits and Systems
Department of Biomedical Engineering
New Jersey Institute of Technology
University Heights
Newark, NJ 07102 USA
Web: http://web.njit.edu/~sahin
Email: sahin@njit.edu

Corresponding author: Mesut Sahin, PhD

Author contributions: Ahmet S. Asan contributed to experimental design, collected the data, and performed signal analysis. Sinan Gok was involved in data collection and drafting the manuscript. Mesut Sahin conceived and designed the experiments, interpreted the data, and reviewed the manuscript.

Abstract

Transcranial electrical stimulation (tES) is rapidly becoming an indispensable clinical tool with its different forms. Animal data are crucially needed for better understanding of the underlying mechanisms of tES. For reproducibility of results in animal experiments, the electric fields (E-Fields) inside the brain parenchyma induced by the injected currents need to be predicted accurately. In this study, we measured the electrical fields in the rat brain perpendicular to the brain surface, *i.e.* vertical electric field (VE-field), when the stimulation electrode was placed over the skin, skull, or dura mater through a craniotomy hole. The E-field attenuation through the skin was a few times larger than that of the skull and the presence of skin substantially reduced the VE-field peak at the cortical surface near the electrode. The VE-field declined much quicker in the gray matter underneath the pial surface than it did in the white matter, and thus the large VE-fields were contained mostly in the gray matter. The transition at the gray/white matter border caused a significant peak in the VE-field, as well as at other local inhomogeneties. A conductivity value of 0.57 S/m is predicted as a global value for the whole brain by matching our VE-field measurements to the field profile given by analytical equations for volume conductors. Finally, insertion of the current return electrode into the shoulder, submandibular, and hind leg muscles had virtually no effects on the measured E-field amplitudes in the cortex underneath the epidural electrodes.

Keywords: transcranial electrical stimulation, electrical field distribution, volume conductor

I. INTRODUCTION

Transcranial electrical stimulation (tES) has emerged as an effective non-invasive technique for modulation of the brain activity in recent years, while the earliest studies date back more than a century (1). In general, the safety of tES and its derivations has now been agreed upon so long as the current is kept below 2mA, although recent reports seem to suggest 4mA as the limit (2). These tES derivations include transcranial direct current stimulation (tDCS), transcranial alternating current stimulation (tACS), and transcranial random noise stimulation (tRNS) (3,4). Despite widespread interest in clinical applications, the exact mechanisms of action for tES are still being investigated.

Aforementioned tES techniques inject weak electrical currents through the brain and presumably cause only subthreshold modulation of the neuronal membrane potentials (5). Early animal studies demonstrated that neuronal firing rates could be modulated by applying direct currents (DC) to the brain (6,7) and the modulatory effects of transcranial DC electric fields were confirmed in human studies (8,9). While the excitatory and inhibitory effects of tDCS are attributed to the direction of the applied current on a larger scale (anodal vs. cathodal) (7,8,10), a more detailed analysis revealed that the primary factor is the position and orientation of the individual neuronal structures relative to the electric field. *In vitro* measurements on rat hippocampal slices showed that the amplitude and delay of the population spikes evoked by orthodromic stimulation were affected linearly by the applied uniform electric fields (11). Furthermore, even small electric fields induced polarization of CA1 pyramidal cells of the hippocampus when applied parallel to the somato-dendritic axis, but failed to do so when applied perpendicularly. Studies on the rat motor cortex slices indicated that somatic polarization was also correlated with the neuronal morphology, and the layer V pyramidal cells were the most sensitive to subthreshold electric fields (12). In general it seems that a realistic estimation of the electric field distribution inside the brain parenchyma is needed as a starting point for accurate interpretations of the neurological impact of the intervention.

69 The electric field can be controlled by adjusting the stimulation current/charge intensity and
70 steered to a certain extent by careful positioning of the extracranial electrodes. Nevertheless, the
71 electrical properties of different tissues that the current passes through play a significant role in
72 distribution of the electric field. Direct *in vivo* measurement of the electric field in human subjects is not
73 an option from a clinical standpoint, thus most investigators resort to computational models in order to
74 approximate the electric field distribution in the human brain under varying stimulation intensities and
75 electrode arrangements. Miranda *et al.* used a spherical head model and estimated that almost 50% of
76 the injected current is shunted through the scalp (13). Datta *et al*. used a more advanced head model
77 where gyri/sulci specificity was defined and predicted that the electric field was concentrated at distinct
78 sites, like the walls of the gyri (14). In summary, tES induced current flow is influenced by several factors
79 including: 1) skull and scalp thicknesses and their compositions, 2) cerebrospinal fluid (CSF) thickness
80 and conductivity, 3) gyri/sulci morphology, 4) electrode size and geometry, and 5) positioning of the
81 stimulating and return electrodes (14,15).

82 In addition to human computational models, tES effects have been studied in animals where the
83 main interests are understanding the underlying cellular and molecular mechanisms, optimizing
84 stimulation protocols, and establishing safety limits. To this end, animal models provide ample
85 opportunities to rapidly develop new tDCS methodologies and measure the outcomes while
86 manipulating the stimulation parameters within a large range that may not be feasible clinically (see (16)
87 for a review). For accurate interpretation of the results from these animal studies, realistic estimates of
88 the induced electric field distribution are needed. Direct measurement of the electric fields in brain
89 tissue goes back to as early as 1950s with experiments carried on anesthetized monkeys (17), although
90 not many follow-up studies reported since then. Chan *et al.* conducted a series of experiments using
91 isolated turtle cerebella, and studied the relationship between the applied fields and the spontaneous
92 neuronal activity (18,19). More recent studies on monkeys (20) and rats (21) also reported electric field

measurements, although restricted either to the cortical surface or a single horizontal plane, respectively.

The tDCS technique can benefit from *in vivo* animal data, which are clearly lacking in the literature, for better understanding of the mechanisms. While the computational models provide a basic understanding of how electrical currents are distributed through the animal brain (22) as much as the human brain, they can lead to unrealistic conclusions if they primarily depend on conductivity measurements gathered from *ex vivo* tissue samples (23). Furthermore, anatomical differences in the brain size and the skin, skull, and CSF thicknesses make it difficult to extrapolate the results of an electric field model developed for one species to another. In this study, we used a rat model to measure the intracerebral voltages at varying depths and horizontal distances from the stimulating electrode. Vertical electric fields were reported for three stimulation conditions in which the anodic electrode was placed over the shaved skin, the skull, and the dura mater. The rat brain was selected in this study due to its common usage as an animal model. We anticipate that the results of this study will provide a reference point for more realistic estimations of the electric field distribution in other studies using the rat model and help to improve the reproducibility of the reported tES effects. Some of the results, such as the shunting effect of the skin and the CSF, agree with modeling predictions, while some others such as the relatively smaller attenuation by the rat skull, the E-field peaks at the white/gray matter border, and insensitivity of the field to the reference electrode location are among the practical findings of this study.

II. METHODS

Animal Surgery

Ten Sprague Dawley rats (250-350g, male) were used in this study for direct measurements of the electric field distribution in the brain parenchyma. This study was carried out in strict accordance with

116 the recommendations in the Guide for the Care and Use of Laboratory Animals of the National Institutes
117 of Health. The protocol was approved by the Institutional Animal Care and Use Committee (IACUC),
118 Rutgers University, Newark, NJ (Protocol Number: 201702616). Anesthesia was induced with 5%
119 isoflurane gas in an induction chamber, maintained by 1-3% isoflurane in 95% oxygen after moving the
120 animals to a stereotaxic frame, and monitored using the toe pinch reflex. All efforts were made to
121 minimize suffering. Blood oxygen level was monitored via a pulse oximeter (NPB-40, Nellcor Puritan
122 Bennet) from the hind paw. Body temperature was measured with a rectal temperature probe (World
123 Precision Instruments-WPI) and regulated with a heating pad (WPI) underneath the animal over the
124 course of surgery. The hair over the head was shaved with an electric shaver and the skin was treated
125 with a depilatory cream to remove the fine hair. The skin was then cleansed with antiseptic solution.

126 **Current Injection over the Skin**:

127 Either 4mm diameter pellet electrodes (EP4, Ag/AgCl, WPI, FL) or 1.5mm diameter helical wire
128 electrodes were used to inject the electric currents. The pellet electrodes are commercially available and
129 thus more common in tES experiments in animals, whereas the helical electrode that is hollow in the
130 center allowed us to make E-field measurements underneath the electrode. The pellet electrode was
131 positioned such that medial edge was juxtaposed to the sagittal suture and the caudal edge to the
132 coronal suture. For helical electrodes, a Ag/AgCl wire with 125µm uncoated thickness (A-M Systems,
133 #786000) was wrapped around a 1.25mm diameter rod 4 times to form a helix with a large surface area
134 and thus a lower impedance. The impedance was confirmed to be below 10kΩ @1kHz in phosphate
135 buffered saline (PBS, Sigma-Aldrich). The helical electrode was filled with conductive gel in the center to
136 ensure good contact with the skin and distribute the current more uniformly at the base of the
137 electrode. The helical electrode was placed with its center positioned 2mm lateral (left or right) from the
138 sagittal suture and 2mm either rostral or caudal to the coronal suture. Another Ag/AgCl wire was
139 inserted to the ipsilateral shoulder muscles as the return (cathodic) electrode for the injected current.

140 Ten monophasic anodic pulses were delivered as a train at 100µA amplitude, 100ms pulse width, and a
141 repetition rate of 4Hz. The amplitude was switched to 200µA at times to increase the signal-to-noise
142 ratio where the recorded amplitudes were too small. In this protocol, substituting pulsed stimulation for
143 DC allowed us to overcome the poor DC response of the metal recording electrodes.

144 A sharp cut was made into the skin with a surgical blade at the edge of the stimulation electrode
145 to expose the skull caudally while leaving the skin underneath the electrode intact (Fig. 1B). Two 1mm
146 diameter craniotomy holes were drilled 2mm and 4mm away from the caudal edge of the stimulation
147 electrode using a micro drill (OmniDrill 35, WPI). A tungsten electrode (0.5 MΩ, TM33B05H, WPI) was
148 inserted into the craniotomy hole to record the induced voltages as a function of depth with respect to
149 another Ag/AgCl reference electrode attached on the skull near the recording electrode using dental
150 acrylic. The dura was punctured with the sharp tip of the tungsten electrode and the first recording was
151 made at the level of the cortical surface (depth=0). Using a 10µ-resolution micromanipulator (Kite-R,
152 WPI), the tungsten electrode was advanced into the brain parenchyma in 0.2mm steps until reaching
153 4mm depth and thereafter in 0.5mm steps up to a depth of 6mm. The procedure was repeated in both
154 craniotomy holes, at 2mm and 4mm horizontal distances from the stimulation electrode. The rising and
155 falling edges of the recorded signals were marked using an automated algorithm in MATLAB (Mathworks
156 Inc.) to quantify the induced voltage amplitudes (see Fig. 2 inset). In some animals, this procedure was
157 repeated on the contralateral side of the brain to obtain an additional set of measurements.

158 **Fig. 1:** Drawings show the three different placements of the stimulation electrode on the rat's
159 head: A) top view. The vertical cross sections of the skin and skull in B, C, and D show the placements of
160 the helical wire stimulation electrode: B) over-the-skin, C) over-the-skull, and D) over-the-dura, and the
161 craniotomy holes for E-field measurements. Tungsten recording electrodes were inserted through the
162 craniotomy holes at center (for over-the-dura stimulation only), and 2mm and 4mm horizontal distances

163 from the stimulation electrode. The pellet electrodes were tested only over-the-skin and skull as shown
164 in B and C.

165 **Current Injection over the Skull**:

166 The skin over the top of the skull was completely removed in this step, mostly in the same animals used
167 above. After removing the periosteum, bone wax was applied to the muscles around the edges and the
168 skull sutures on top to stop bleeding. The stimulation electrode (pellet or helical wire) was placed onto
169 the skull (Fig. 1C) at the same coordinates used with over-the-skin electrodes measured with respect to
170 the *bregma*. The voltage measurements were made following the same procedure above with slight
171 repositioning of the tungsten electrode in the same craniotomy holes in order to avoid damaged tissue
172 from the previous penetration.

173 **Current Injection over the Dura**:

174 A 2mm craniotomy hole was made at the coordinates of the stimulation electrode to inject the current
175 directly through the dura (Fig. 1D). A helical wire electrode (1.5mm diam.) was placed about 0.5mm
176 above the dura mater and anchored to the edge of the skull hole with small amounts of cyanoacrylate
177 glue and the hole was filled with normal saline. The distances between the caudal edge of the helical
178 electrode and recording holes were kept at 2mm and 4mm as before. With the helical electrodes, an
179 additional set of voltage recordings were made by inserting the tungsten electrode through the center
180 of the stimulation electrode.

181 Finally, in order to investigate the effect of the current return electrode position, the Ag/AgCl
182 wire inserted to the ipsilateral shoulder muscles was moved to the contralateral shoulder, the hind leg,
183 and the submandibular muscles via needle insertions. The voltage measurements were repeated near
184 the cortex and at various depths with the recording electrode in the center of the helical electrode for
185 these four different positioning of the current return electrode for comparison.

Data Collection and Analysis:

The signals were collected in a large Faraday cage and first amplified by a gain of 100 (Model 1700, A-M Systems, WA) with filters setting of 10 Hz–10 kHz, and then sampled at 25kHz through a National Instruments data acquisition board (PCI 6071) controlled by custom-designed MATLAB codes. Stimulus-triggered averaging (STA) was used (N=10) to suppress the background neural activity and other sources of random noise. The averaged signal was further band-pass filtered in MATLAB (10 Hz – 1 kHz) before analyzing. Voltage transitions within 2ms window around the rising edge of the square pulses were taken as the induced voltage at the corresponding depth. The first derivative of the voltage data with respect to depth was computed as the electric field (E-field). All field measurements were made exclusively in the vertical direction (VE-field) in this study. Horizontal E-field measurements would require derivation of the voltage measurements made through different brain penetrations and lead to large calculation errors due to even slight changes in the absolute value of the voltages measured, which could easily occur from repositioning of the recording reference electrode between penetrations.

Comparison with Theoretical Models

The resistance of a monopolar disk electrode at the surface of a semi-infinite, homogeneous, and isotropic medium was first derived by Newman (24) as a function of the electrode radius (a), and the conductivity of the medium (σ). The potential at the surface is found as $Vo = I/(4\sigma a)$, where I is the electrode current. Wiley and Webster then solved the Laplace's equation for the voltage distribution inside the semi-infinite volume conductor for a similar disk electrode (25). By substituting zero for the horizontal axis r in their equation, we find the voltage profile at the electrode center, which starts from Vo at z=0 and declines with increasing values of the vertical axis (z) according to the equation $(2Vo/\pi)\sin^{-1}(a/\sqrt{z^2+a^2})$. The VE-field, however, decreases as a function of $\varphi = -(2Vo/\pi)(a/z^2 + a^2)$, which can be found easily by differentiating the voltage equation with respect to z, and the peak

209 value of the VE-field at the surface (*z*=0, r=0) is $\varphi = -2Vo/(\pi a)$ or $\varphi = I/(2\pi\sigma a^2)$. We fit the VE-field
210 equation to our data collected with the epidural placement of the electrode at its center while leaving
211 *Vo* as a free parameter (Fig. 2, center). The *Vo* value that fits the experimental data best for r=0 was also
212 used to plot the VE-field equation at r=2mm and r=4mm from the edge of the stimulation electrode in
213 Fig. 2 (2mm and 4mm). The VE-field is shown as a 2D heat plot in Fig. 3 for comparison with the
214 experimental data and will be discussed at the end.

215 **Fig. 2:** Voltage (top row) and VE-field (bottom row) measurements made with epidural (as in Fig.
216 1D) placement of the Ag/AgCl helical wire stimulation electrode with 1.5 diam. Top Row Left to Right:
217 Voltage measurements made with respect to a reference on the skull and via penetrations at the center,
218 and 2mm and 4mm from the edge of the helical electrode. Seven sets of measurements were collected
219 in five animals. In two sets, the voltage was measured at a fewer points below 3mm of depth. In such
220 cases, exponential interpolation was utilized to estimate the missing voltage values. The inset depicts
221 how the voltage amplitude (a) measurements were made at the rising edge of the recorded waveforms.
222 Bottom Row: The mean of the vertical E-fields calculated by differentiating the voltage measurements
223 shown in the top row for each penetration separately. The shaded areas indicate ± standard error. The
224 black solid line is the VE-field predicted by the analytical equation derived by Wiley & Webster (24) that
225 provided the best fit, *i.e.* highest coefficient of determination (R2), when *Vo* at V(r=0, z=0) is set to
226 58.3mV. For 2mm and 4mm penetrations, the analytical equation was evaluated (solid black lines) using
227 the same *Vo* value for consistency.

228 **Fig. 3:** Vertical E-field distribution as a heat plot on a logarithmic scale. The left panel was
229 obtained by linear interpolation of the measurements presented in Fig. 2 and reflected over the vertical
230 axis in the middle. The right panel is the predicted VE-field by the analytical equations of Wiley &
231 Webster. Depth=0 corresponds to the surface of the cortex.

232 **III. RESULTS**

233 **VE-Fields with Epidural Injection of Current**

234 The peak-to-peak voltage induced by the current pulse was measured as a function of depth down to
235 6mm from the dura surface (Fig. 2, top row) at the center of the helix, and 2mm and 4mm away
236 horizontally from the stimulation electrode (see Fig. 1D). Vertical electrical fields (VE-fields) were
237 computed by differentiating the raw voltage measurements without any filtering or curve fitting, and
238 averaged across the animals (Fig. 2, bottom row). Note that the vertical offset in the voltage plots of the
239 top row do not carry any significance since they can vary between animals depending on where the
240 recording reference electrode is placed along the current pathways between the stimulation and the
241 return electrodes. The voltage curves decline sharply under the stimulation electrode with maximum
242 values underneath the dura (depth=0mm), as expected. The VE-field was also maximum under the
243 stimulation electrode (center, depth=0mm) near the cortex, declined exponentially, and lost more than
244 75% of its strength by 2mm below the stimulation electrode and further decreased down to negligible
245 levels by 6mm. The analytical equation by Wiley and Webster (see methods) was evaluated and fit to
246 the VE-field by using *Vo* as the free parameter. The analytical formula provided a good-fit (R^2=0.92)
247 including the initial plateau near the cortical surface for *Vo*=58.3mV. As the recording electrode was
248 moved horizontally to 2mm and 4mm away from the stimulation site, the VE-field decline near the
249 surface became sharper and an elevation appeared at deeper levels. The initial sharp decline was not
250 predicted by the analytical equation since the semi-infinite model assumes a non-conductive medium
251 above the surface and a zero vertical current at the boundary. The band of large VE-fields extending
252 horizontally underneath the surface can also be appreciated from the heat plot of Fig. 3A. Interestingly,
253 for all penetrations (center, 2, 4mm) there seems to be a peak in the E-field near or a little above the
254 2mm mark, which may indicate a sharp change in tissue conductivity, e.g. from gray matter to white
255 matter. The analytical equations fail to predict the VE-field amplitudes, in general, at 2mm and 4mm

from the stimulation electrode with the same *Vo* used at center penetration. Thus, the VE-fields expand more in the horizontal direction than predicted.

Comparison of VE-Fields with Current Injections over the Skin, Skull, and Dura

Figure 4 compares the VE-fields with three different placements of the helical electrode; over the skin, skull, and dura. The epidural stimulation produces the largest electric field intensities in the brain parenchyma while epidermal placement produces the lowest intensity, as expected, both at 2mm and 4mm horizontal locations from the electrode. Note that for over-the-skin and skull placements of the stimulation electrode the E-fields measurements were not in the center of the electrode in order not to disturb the intactness of the skin or skull with a penetration hole. The skin attenuated the VE-field (or shunted the electric currents) to a much larger degree than the skull, as seen with penetrations both at 2mm and 4mm horizontal locations from the stimulation electrode. The over-the-skin placement did not produce an exponentially decreasing VE-field profile by depth as the other two placements of the stimulation electrode, and the VE-fields measured at the cortical surface (depth=0) were about an order of magnitude smaller. The skin thickness was measured at the end of the experiment and found to be around 0.5mm under the stimulation electrode.

Fig. 4: Comparison of VE-fields for three different placements of the helical wire electrode over the skin, skull, and dura mater. Measurements are repeated at 2mm (left) and 4mm (right) horizontal distances from the edge of the helical electrode. The averages of (n) measurement sets are plotted (solid lines) and the standard errors are shown as shaded areas.

The VE-fields were also compared with larger Ag/AgCl pellet electrodes (diam.=4mm) placed either over the skin or skull (Fig. 5). At a horizontal distance of 2mm from the edge of the pellet electrode, the presence of skin attenuated the electric fields by 3-4 times, similar to the smaller helical electrodes, but the VE-field decline was sharper by depth with the pellet electrode compared to the

279 smaller helical electrodes. This was probably because the pellet electrode had a larger diameter and the
280 2mm from the edge was actually further away from the electrode center compared to the helical
281 electrodes. That the VE-field decline within the first mm of depth becoming sharper as the penetrations
282 move horizontally was also observed with the helical electrode (Fig. 2). The VE-field bump around 1.5-
283 2mm depth was observed consistently in these plots as well. For both skin and skull placements of the
284 stimulation electrode, the measurements at 4mm were about a few times smaller than those at 2mm.

285 **Fig. 5:** Comparison of VE-fields for two different placements of the large pellet electrode; over
286 the skin and skull. Details are same as in Fig. 4.

287 **Location of the Current Return Electrode**

288 Lastly, we investigated how the location of the stimulation reference electrode affects the electric field
289 strength in two rats. In the previous experiments, a Ag/AgCl wire inserted into the ipsilateral shoulder
290 was used as the current return electrode (cathode). For this experiment, three alternative sites were
291 tested for the cathodic electrode: the contralateral shoulder, the submandibular muscles, and the
292 ipsilateral hind limb. The epidural stimulation experiments with the helical wire electrodes were
293 repeated against these reference electrode placements and the VE-fields as the difference of the voltage
294 between the depths of 0.6-2.0mm were measured in nine different craniotomy holes (4 and 5 holes in
295 two rats) as the stimulus was applied through the same hole. The maximum deviation from the ipsi-
296 shoulder measurement was less than 1.36% with any of the new reference points. None of the VE-field
297 measurement sets made at various depths from 0.6 to 2mm (N=5) against the novel reference points
298 were significantly different from that of the set against the ipsi-shoulder electrode (paired t-test, $p>0.5$).

299 **IV. DISCUSSION**

300 **E-field Attenuation by Skin and Skull**

301 The skin thickness changes around the head and rodents are no exception to this rule. Because of the
302 compression we applied to hold the electrode down firmly on the skin, the skin thickness decreased
303 under the stimulation electrode during the course of the experiment and found to be ~0.5mm at the
304 end. The skin had to be removed also caudal to the stimulation electrode to make craniotomy holes at
305 the recording points. Hence, we can only make general remarks about the skin effects on the E-field
306 measurements in the face of these sources of variability and practical limitations. About a four-fold
307 decrease occurred in the VE-field when the electrode was placed over the skin as opposed to the skull
308 surface. The average skull thickness was measured to be ~0.5mm (N=5). In agreement with this data,
309 Vöröslakos et al. reported that transcutaneous stimulation generated several-fold weaker electric fields
310 compared to subcutaneous stimulation in rats (21). There was a relatively small loss of electric field
311 intensity when the helical electrode was moved from the dural surface to the skull surface in our data.

312 With over-the-skin electrodes and 100µA current injection, the vertical electric field drops down
313 to ~1mV/mm at 2mm and 4mm from the stimulation electrode (Fig. 4). Terzulo and Bullock reported
314 that the firing frequency of neurons can be modulated by voltage gradients as low as 1mV/mm (10),
315 which is also the lower bound indicated by rodent studies (21,26). The large variability in the skin
316 thickness and the high conductivity of skin can make the results with epidermal montage highly
317 unpredictable. Therefore, placing the electrode over the skull would be a reasonable compromise to
318 mitigate the effects of current shunting by the skin and to improve the focality of stimulation, while still
319 avoiding large E-field peaks as they occur with epidural stimulation.

320 We did not measure the VE-field at the electrode center with over-the-skull electrodes. The
321 epidural stimulations in Fig. 2 show that the VE-field under the electrode decreases by about a factor of
322 two from the electrode center to 2mm off the edge. If we can extrapolate from over-the-skull
323 stimulations in Fig. 4 at 2mm, the VE-field under the electrode should be about 25mV/mm at the cortical
324 level. The current density at electrode-tissue interface is 56.6 A/m^2 for the helical electrode. If we scale

325 the above VE-field value for the current density (142.9 A/m^2) used by Jackson et al. (27), the result (63
326 mV/mm) is about 50% higher than the cortical electric fields (42 V/m or 42 mV/mm) predicted in the rat
327 using finite element modeling in their publication. This discrepancy may be due to the differences in the
328 assumed thicknesses and conductivities of the skull and CSF in the model.

329 **Non-Homogeneity of the Brain**

330 That the skull resistivity was much higher than that of the skin and brain tissue was first demonstrated
331 by early intracerebral voltage measurement studies in human cadavers (28) and anesthetized monkeys
332 (17). Hayes predicted that the high conductivity of the skin and scalp would tend to make the electrical
333 fields more uniform inside the brain. Our data with over-the-skin stimulation does not have the
334 exponentially decaying profile by depth as in over the skull and dura stimulations, and thus agrees with
335 Hayes' prediction in general. A particular aspect to note is the VE-field peak that occurred consistently at
336 around 1.5-2mm depths in most plots where the gray matter transitions into the white matter and thus
337 a significant change in local conductivity is expected. The lower conductivity of the white matter seems
338 to cause an elevation in the VE-field at the border of the two regions. The fact that the VE-field decline
339 in the gray matter is sharper at 2mm and 4mm horizontal locations than at the electrode center (Fig. 2)
340 must, however, be due to the higher conductivity of the cerebrospinal fluid near the surface, rather than
341 the gray/white matter conductivity differences.

342 **Electrode Size**

343 The electrode size is the primary factor that can help focalize the induced E-field and the affected
344 volume of tissue (29). Smaller size electrodes require less total current than larger electrodes to induce
345 the same current density at a fixed target point in the brain (30). However the current density at the
346 electrode surface is higher than that of the larger electrodes (31). We did not specifically compare the
347 two different electrode sizes we had due to insufficient statistical power in the data.

348 **Monopolar vs. Bipolar Montages**

349 Repositioning the return electrode from the shoulder to other muscles around the body introduced
350 changes smaller than 1.36% in the VE-field. This confirms the results reported from finite element
351 models that the voltage profile near the anodic electrode is more or less the same with the monopolar
352 montage so long as the large surface return electrode is placed far enough from the anode. The field
353 steering effect begins to occur when the return electrode is brought near the stimulation electrode,
354 hence approximating a bipolar montage (32,33). Moliadze et al. (34) reported that the stimulation
355 effects can significantly change depending on the distance between the stimulation electrodes, even for
356 the extracephalic placement of the return electrode (*e.g*. ipsilateral upper arm vs. ipsilateral forearm) in
357 the human. This result is surprising since the current flow patterns should not be affected by the
358 position of the return electrode as long as it is on the same arm. The sensitivity of the results to the
359 location of the return electrode may be higher with epidermal placement of the electrodes due to
360 currents flowing through the highly conductive skin. A practical point raised by our data is that the
361 Ag/AgCl wires deinsulated for several mm at the end and inserted into a muscle can conveniently serve
362 as a return electrode, replacing the large surface transcutaneous electrodes used in other studies
363 (35,36).

364 That the E-field declines sharply by distance with monopolar montages is advantageous for
365 spatial selectivity if the targeted neural structures are near the brain surface but makes it difficult to
366 achieve significant E-fields at deeper brain regions without causing extreme electric fields near the
367 surface. Attempts to focus the electric field at subcortical brain regions using multiple electrodes will
368 have to deal with this challenge. Horizontal E-field can be maximized using bipolar montages by placing
369 both the cathode and the anode around the head on the sides, if the targeted neural structures are
370 inside the cortical sulci where the somato-dendritic axis of the neurons is oriented horizontally. A recent
371 paper (21) proposed both spatial focusing and time-multiplexing of the stimulus currents via multiple

372 dipoles in order to maximize the horizontal E-field at a focal point inside the brain by taking advantage
373 of the slow time constant of the cellular membranes at subthreshold potentials. While the tES methods
374 enjoy the benefits of being non-invasive, the challenge of focalization may remain as the main
375 disadvantage of the technique in the long run.

376 **Stimulation Waveform**

377 In our protocol, substituting DC with pulsed stimulation allowed us to overcome the poor DC response
378 of the tungsten recording electrodes. The brain tissue can be treated primarily as a resistive medium
379 hence the recorded amplitudes to be independent of frequency, up to 10kHz and even higher ranges
380 (13,37) owing to the "quasi-static approximation". Thus, our amplifier's high cutoff (f_c) was set to 10kHz,
381 which has corresponding rise time of 15.9µs ($t_r = 1/2\pi f_c$) for a first-order filter. We took the amplitude
382 measurements 1ms after the pulse transition, allowing several rise times for the signals to stabilize while
383 still being much shorter than the time constant imposed by the lower cutoff frequency of the amplifier
384 ($t_r = 15.9ms$, 10Hz) .

385 A sinusoidal waveform at a constant frequency (e.g. 1kHz) could also be used for the stimulus
386 current in this study instead of rectangular pulses. A stimulus waveform with a single frequency would
387 overcome the bandwidth limitations of the metal recording electrodes and the amplifier, which
388 attenuates the harmonics of a rectangular waveform to different degrees and distorts the recorded
389 waveforms. The advantage of the rectangular waveform, however, is that any mechanical disturbance to
390 the electrode tip during penetration manifests itself not only as a change in the measured amplitudes
391 but also as a distortion in the waveform, and thus alerts the experimenter about the quality of the
392 signals. With sinusoidal waveforms only the signal amplitude would change, which could escape the
393 attention of the experimenter and lead to significant miscalculations of the E-field.

394 **Comparison with Theoretical Models**

395 Despite the fact that Wiley & Webster equation (25) assumes a homogeneous medium, and does not
396 account for the impedance of the electrode-electrolyte interface and the current redistribution across
397 the electrode surface due to amplitude and frequency dependency of the interface (38), it provides a
398 reference point for comparison. The simplicity of using an analytical equation instead of building
399 complicated models can be much more practical for quick estimations of the E-field underneath a
400 monopolar electrode if that is all that is needed. Comparison of the experimental data with the
401 theoretical model in 2D (Fig. 3) reveals some fundamental similarities but also significant differences.
402 Both plots show that the largest VE-fields occur under the electrode, but the experimental VE-field
403 diminishes within the gray matter for the most part, subsiding to negligible levels in the white matter. In
404 the experimental data the VE-field spreads more in the horizontal direction near the surface most likely
405 due to the high conductivity of the CSF, and perhaps that of the gray matter also to a degree. The
406 theoretical plot assumes a non-conductive medium above the brain and does not account for the
407 presence of the skull. In addition, there are clearly regions of varying conductivities in the experimental
408 data that cause inhomogeneities in the electric field. Lastly, the VE-peaks at the electrode edges that are
409 suggested by the earlier analytical models (25) were not observed in the experimental data. This may be
410 because of the distance (~0.5mm) allowed between the electrode surface and the brain cortex in our
411 setup, or the spatial smoothing of the E-field peaks may be explained partially by the presence of the
412 electrode-electrolyte interface as predicted by more advanced models (38).

413 **Practical Considerations**

414 The surface area of the electrode that is in contact with tissue primarily determines the E-field strength
415 in the vicinity of the electrode. Therefore, epidural placement of the stimulation electrode may lead to
416 large variations in the E-fields in the cortex if the electrode moves even by very small amounts. If the
417 electrode contact area with the cortex is well defined, the simple analytical equations (25) can become
418 very useful for predicting the potential and the VE-field underneath the electrode. The equation for the

419 VE-field at the surface (*z*=0, r=0) is $\varphi = -2Vo/(\pi a)$. For *Vo* value that gives the best fit with this
420 equation to our data was found to be 58.3mV. Assuming a homogenous medium, an overall conductivity
421 value of 0.57 S/m can be found by substituting this value of *Vo* into the Newman equation ($Vo =$
422 $I/(4\sigma a)$), which is about three times higher than the commonly used conductivity for the brain (0.2
423 S/m) most likely due to the high conductivity of the CSF (1.65 S/m) (39). For a known electrode
424 diameter and current, one can use this *modified* conductivity value to estimate the VE-field peak
425 underneath the epidural electrodes. Having an accurate prediction for the vertical E-field near the
426 surface, where most of the cortical neurons are found in an animal with a lissencephalic brain like the
427 rat, can prove to be useful when direct measurements of the field is not possible.

428 The current distribution across the disk electrodes is predicted to suffer from edge-effects by
429 earlier models (25). Inclusion of the electrode-electrolyte interface into the model produces a more
430 uniform current profile across the surface, although the effect is amplitude and frequency dependent
431 (38). The choice of the electrode material thus is crucial to minimize the electrode-electrolyte
432 impedance and improve reproducibility. In order to prevent the edge-effects from influencing the E-
433 field distribution inside the brain, the stimulation electrode can be kept at a distance from the
434 superficial layers of the cortex. The skull can serve as a spacer in this case. The disk electrode can be
435 attached onto the skull at reproducible stereotaxic coordinates and the top of the electrode can be
436 covered with some nonconductive material to prevent current spreading through the skin. The skull
437 thickness at the point of electrode placement can be standardized to a degree by controlling the
438 weight/age of the animal. Alternatively, one can also make a craniotomy hole and fill it with conductive
439 gel or isotonic saline and position the stimulation electrode at a known distance above the cortex as we
440 did with epidural stimulations. Because normal saline has a conductivity (1.65 S/m) that is about eight
441 times higher than that of the brain (0.2 S/m), the stimulation electrode may electrically be assumed to
442 be at the cortex/saline interface for practical purposes. The highly conductive saline may however be

replaced with encapsulation tissue by time in chronic implants. For most reproducible results, the E-field should be measured directly inside the tissue in each animal separately if this can be done without disturbing the intactness of the neurons or the E-field itself.

V. CONCLUSIONS

This paper provides experimental data as a reference study for more realistic estimates of the electric fields induced in the rat brain during tES studies. The skin attenuates the electric field much more strongly than the skull and causes the current spread more uniformly inside the skull. For focal stimulation, it may be best to place the stimulation electrode on the skull to avoid the skin effect. The electrical field perpendicular to the cortex decreases exponentially near the surface and loses most of its strength within 2mm into the brain underneath the electrode and within 1mm of depth off of the electrode edge. A 100µA current injected through a 1.5mm over-the-skull electrode is predicted to generate ~25mV/mm at the cortical surface. For epidural placements of the stimulation electrode through a craniotomy hole, a modified value of 0.57 S/m for the brain conductivity can be assumed to estimate the voltage at the cortical surface using the volume conductor equations. Significant E-field peaks occur in the brain parenchyma, most likely due to local conductivity changes, especially at the gray/white matter border. These large fluctuations in the E-field measurements show that the homogeneous volume conductor assumption is too simplistic for modeling the local effects of the injected current.

ACKNOWLEDGMENTS

Supported by NIH/NINDS Grant No: R21 NS101386.

463 **REFERENCES**

464 1. Priori A. Brain polarization in humans: A reappraisal of an old tool for prolonged non-invasive
465 modulation of brain excitability [Internet]. Vol. 114, Clinical Neurophysiology. Elsevier; 2003
466 [cited 2018 May 14]. p. 589–95. Available from:
467 https://www.sciencedirect.com/science/article/pii/S1388245702004376?via%3Dihub

468 2. Chhatbar PY, Chen R, Deardorff R, Dellenbach B, Kautz SA, George MS, et al. Safety and
469 tolerability of transcranial direct current stimulation to stroke patients – A phase I current
470 escalation study. Brain Stimul [Internet]. 2017 May 1 [cited 2018 Aug 14];10(3):553–9. Available
471 from: https://www.sciencedirect.com/science/article/pii/S1935861X17306149?via%3Dihub

472 3. Bikson M, Grossman P, Thomas C, Zannou AL, Jiang J, Adnan T, et al. Safety of Transcranial Direct
473 Current Stimulation: Evidence Based Update 2016 [Internet]. Vol. 9, Brain Stimulation. Elsevier;
474 2016 [cited 2018 Feb 17]. p. 641–61. Available from: https://www-sciencedirect-
475 com.libdb.njit.edu:8443/science/article/pii/S1935861X16301401

476 4. Antal A, Alekseichuk I, Bikson M, Brockmöller J, Brunoni AR, Chen R, et al. Low intensity
477 transcranial electric stimulation: Safety, ethical, legal regulatory and application guidelines. Clin
478 Neurophysiol [Internet]. 2017 Sep 1 [cited 2018 Nov 19];128(9):1774–809. Available from:
479 https://www.sciencedirect.com/science/article/pii/S1388245717302122

480 5. Woods AJ, Antal A, Bikson M, Boggio PS, Brunoni AR, Celnik P, et al. A technical guide to tDCS,
481 and related non-invasive brain stimulation tools. Clin Neurophysiol [Internet]. 2016 Feb [cited
482 2018 Feb 12];127(2):1031–48. Available from: http://www.ncbi.nlm.nih.gov/pubmed/26652115

483 6. Creutzfeldt OD, Fromm GH, Kapp H. Influence of transcortical d-c currents on cortical neuronal
484 activity. Exp Neurol [Internet]. 1962 Jun 1 [cited 2018 May 24];5(6):436–52. Available from:

485 https://www.sciencedirect.com/science/article/pii/0014488662900560

486 7. Bindman LJ, Lippold OCJ, Redfearn JWT. The action of brief polarizing currents on the cerebral
487 cortex of the rat (1) during current flow and (2) in the production of long-lasting after-effects. J
488 Physiol [Internet]. 1964 Aug 1 [cited 2018 Jan 29];172(3):369–82. Available from:
489 http://www.ncbi.nlm.nih.gov/pubmed/14199369

490 8. Nitsche MA, Paulus W. Excitability changes induced in the human motor cortex by weak
491 transcranial direct current stimulation. J Physiol [Internet]. 2000 Sep 15;527 Pt 3(3):633–9.
492 Available from: http://www.ncbi.nlm.nih.gov/pubmed/10990547

493 9. Lang N, Siebner HR, Ward NS, Lee L, Nitsche MA, Paulus W, et al. How does transcranial DC
494 stimulation of the primary motor cortex alter regional neuronal activity in the human brain? Eur J
495 Neurosci [Internet]. 2005 Jul 21 [cited 2018 Feb 12];22(2):495–504. Available from:
496 http://www.ncbi.nlm.nih.gov/pubmed/16045502

497 10. Terzuolo CA, Bullock TH. Measurement of imposed voltage gradient adequate to modulate
498 neuronal firing. Proc Natl Acad Sci U S A [Internet]. 1956 Sep 1 [cited 2018 May 14];42(9):687–94.
499 Available from: http://www.ncbi.nlm.nih.gov/pubmed/16589932

500 11. Bikson M, Inoue M, Akiyama H, Deans JK, Fox JE, Miyakawa H, et al. Effects of uniform
501 extracellular DC electric fields on excitability in rat hippocampal slices in vitro. J Physiol [Internet].
502 2004 May 1 [cited 2018 Feb 14];557(1):175–90. Available from:
503 http://doi.wiley.com/10.1113/jphysiol.2003.055772

504 12. Radman T, Ramos RL, Brumberg JC, Bikson M. Role of cortical cell type and morphology in
505 subthreshold and suprathreshold uniform electric field stimulation in vitro. Brain Stimul
506 [Internet]. 2009 Oct 1 [cited 2018 Feb 12];2(4):215–228.e3. Available from: https://www-

507 sciencedirect-com.libdb.njit.edu:8443/science/article/pii/S1935861X09000424

508 13. Miranda PC, Lomarev M, Hallett M. Modeling the current distribution during transcranial direct
509 current stimulation. Clin Neurophysiol [Internet]. 2006 Jul [cited 2018 Feb 17];117(7):1623–9.
510 Available from: https://ac-els-cdn-com.libdb.njit.edu:8443/S1388245706001726/1-s2.0-
511 S1388245706001726-main.pdf?_tid=spdf-bcaa1334-c0a1-4d41-ace8-
512 3264c5f7dbcf&acdnat=1518917934_be472fc3bac6d2140f8f7e1c73e4eb56

513 14. Datta A, Bansal V, Diaz J, Patel J, Reato D, Bikson M. Gyri-precise head model of transcranial
514 direct current stimulation: Improved spatial focality using a ring electrode versus conventional
515 rectangular pad. Brain Stimul [Internet]. 2009 Oct [cited 2018 May 29];2(4):201–207.e1. Available
516 from: http://www.ncbi.nlm.nih.gov/pubmed/20648973

517 15. Opitz A, Paulus W, Will S, Antunes A, Thielscher A. Determinants of the electric field during
518 transcranial direct current stimulation. Neuroimage. 2015 Apr;109:140–50.

519 16. Jackson MP, Rahman A, Lafon B, Kronberg G, Ling D, Parra LC, et al. Animal models of transcranial
520 direct current stimulation: Methods and mechanisms. Clin Neurophysiol [Internet]. 2016 Nov
521 [cited 2018 Feb 12];127(11):3425–54. Available from:
522 http://www.ncbi.nlm.nih.gov/pubmed/27693941

523 17. Hayes KJ. The current path in electric convulsion shock. Arch Neurol Psychiatry [Internet]. 1950
524 Jan 1 [cited 2018 Feb 20];63(1):102–9. Available from:
525 http://archneurpsyc.jamanetwork.com/article.aspx?doi=10.1001/archneurpsyc.1950.02310190108008

527 18. Chan CY, Nicholson C. Modulation by applied electric fields of Purkinje and stellate cell activity in
528 the isolated turtle cerebellum. J Physiol [Internet]. 1986 Feb [cited 2018 Jun 8];371:89–114.

Available from: http://www.ncbi.nlm.nih.gov/pubmed/3701658

19. Chan CY, Hounsgaard J, Nicholson C. Effects of electric fields on transmembrane potential and excitability of turtle cerebellar Purkinje cells in vitro. J Physiol [Internet]. 1988 Aug [cited 2018 Jun 8];402:751–71. Available from: http://www.ncbi.nlm.nih.gov/pubmed/3236254

20. Opitz A, Falchier A, Yan C-G, Yeagle EM, Linn GS, Megevand P, et al. Spatiotemporal structure of intracranial electric fields induced by transcranial electric stimulation in humans and nonhuman primates. Sci Rep [Internet]. 2016 Nov 18 [cited 2018 Jan 29];6(1):31236. Available from: http://www.nature.com/articles/srep31236

21. Vöröslakos M, Takeuchi Y, Brinyiczki K, Zombori T, Oliva A, Fernández-Ruiz A, et al. Direct effects of transcranial electric stimulation on brain circuits in rats and humans. Nat Commun [Internet]. 2018 Dec 2 [cited 2018 Apr 14];9(1):483. Available from: http://www.nature.com/articles/s41467-018-02928-3

22. Gasca F, Marshall L, Binder S, Schlaefer A, Hofmann UG, Schweikard A. Finite element simulation of transcranial current stimulation in realistic rat head model. In: 2011 5th International IEEE/EMBS Conference on Neural Engineering [Internet]. IEEE; 2011 [cited 2018 Jun 25]. p. 36–9. Available from: http://ieeexplore.ieee.org/document/5910483/

23. Huang Y, Liu AA, Lafon B, Friedman D, Dayan M, Wang X, et al. Measurements and models of electric fields in the in vivo human brain during transcranial electric stimulation. Elife [Internet]. 2017 Feb 7 [cited 2018 May 8];6:e18834. Available from: https://elifesciences.org/articles/18834

24. Newman J. Resistance for Flow of Current to a Disk. J Electrochem Soc [Internet]. 1966 May 1 [cited 2018 Aug 14];113(5):501. Available from: http://jes.ecsdl.org/cgi/doi/10.1149/1.2424003

25. Wiley JD, Webster JG. Analysis and control of the current distribution under circular dispersive

551 electrodes. IEEE Trans Biomed Eng [Internet]. 1982 May [cited 2018 Jun 21];29(5):381–5.
552 Available from: http://ieeexplore.ieee.org/document/4121424/

553 26. Ozen S, Sirota A, Belluscio MA, Anastassiou CA, Stark E, Koch C, et al. Transcranial electric
554 stimulation entrains cortical neuronal populations in rats. J Neurosci [Internet]. 2010 Aug 25
555 [cited 2018 Jan 29];30(34):11476–85. Available from:
556 http://www.ncbi.nlm.nih.gov/pubmed/20739569

557 27. Jackson MP, Truong D, Brownlow ML, Wagner JA, McKinley RA, Bikson M, et al. Safety parameter
558 considerations of anodal transcranial Direct Current Stimulation in rats. Brain Behav Immun
559 [Internet]. 2017 Aug 1 [cited 2018 Nov 19];64:152–61. Available from:
560 https://www.sciencedirect.com/science/article/pii/S0889159117301101

561 28. Smitt JW, Wegener CF. ON ELECTRIC CONVULSIVE THERAPY: with particular regard to a parietal
562 application of electrodes, controlled by intracerebral voltage measurements1. Acta Psychiatr
563 Scand [Internet]. 1944 Dec 31 [cited 2018 Jun 1];19(3–4):529–49. Available from:
564 http://doi.wiley.com/10.1111/j.1600-0447.1944.tb04586.x

565 29. Nitsche MA, Doemkes S, Karakose T, Antal A, Liebetanz D, Lang N, et al. Shaping the Effects of
566 Transcranial Direct Current Stimulation of the Human Motor Cortex. J Neurophysiol [Internet].
567 2007 Apr [cited 2018 Jun 25];97(4):3109–17. Available from:
568 http://www.physiology.org/doi/10.1152/jn.01312.2006

569 30. Faria P, Hallett M, Miranda PC. A finite element analysis of the effect of electrode area and inter-
570 electrode distance on the spatial distribution of the current density in tDCS. J Neural Eng
571 [Internet]. 2011 Dec 1 [cited 2018 Jun 25];8(6):066017. Available from:
572 http://stacks.iop.org/1741-
573 2552/8/i=6/a=066017?key=crossref.83f3d9681922067b4b8b72fa29d78dd5

574 31. Miranda PC, Faria P, Hallett M. What does the ratio of injected current to electrode area tell us
575 about current density in the brain during tDCS? Clin Neurophysiol [Internet]. 2009 Jun 1 [cited
576 2018 May 14];120(6):1183–7. Available from:
577 https://www.sciencedirect.com/science/article/pii/S1388245709003046?via%3Dihub

578 32. Bikson M, Datta A, Rahman A, Scaturro J. Electrode montages for tDCS and weak transcranial
579 electrical stimulation: Role of "return" electrode's position and size. Clin Neurophysiol [Internet].
580 2010 Dec 1 [cited 2018 May 8];121(12):1976–8. Available from:
581 https://www.sciencedirect.com/science/article/pii/S1388245710004803?via%3Dihub

582 33. Noetscher GM, Yanamadala J, Makarov SN, Pascual-Leone A. Comparison of Cephalic and
583 Extracephalic Montages for Transcranial Direct Current Stimulation—A Numerical Study. IEEE
584 Trans Biomed Eng [Internet]. 2014 Sep [cited 2018 Nov 22];61(9):2488–98. Available from:
585 http://ieeexplore.ieee.org/document/6847106/

586 34. Moliadze V, Antal A, Paulus W. Electrode-distance dependent after-effects of transcranial direct
587 and random noise stimulation with extracephalic reference electrodes. Clin Neurophysiol
588 [Internet]. 2010 Dec 1 [cited 2018 Nov 2];121(12):2165–71. Available from:
589 https://www.sciencedirect.com/science/article/pii/S1388245710004815?via%3Dihub

590 35. Tanaka T, Takano Y, Tanaka S, Hironaka N, Kobayashi K, Hanakawa T, et al. Transcranial direct-
591 current stimulation increases extracellular dopamine levels in the rat striatum. Front Syst
592 Neurosci [Internet]. 2013 Apr 11 [cited 2018 Nov 19];7:6. Available from:
593 http://journal.frontiersin.org/article/10.3389/fnsys.2013.00006/abstract

594 36. Dockery CA, Liebetanz D, Birbaumer N, Malinowska M, Wesierska MJ. Cumulative benefits of
595 frontal transcranial direct current stimulation on visuospatial working memory training and skill
596 learning in rats. Neurobiol Learn Mem [Internet]. 2011 Oct 1 [cited 2018 Nov 19];96(3):452–60.

Available from: https://www.sciencedirect.com/science/article/pii/S1074742711001298

37. Ruffini G, Wendling F, Merlet I, Molaee-Ardekani B, Mekonnen A, Salvador R, et al. Transcranial current brain stimulation (tCS): models and technologies. IEEE Trans Neural Syst Rehabil Eng [Internet]. 2013 May [cited 2018 May 8];21(3):333–45. Available from: http://ieeexplore.ieee.org/document/6290404/

38. Cantrell DR, Inayat S, Taflove A, Ruoff RS, Troy JB. Incorporation of the electrode–electrolyte interface into finite-element models of metal microelectrodes. J Neural Eng [Internet]. 2008 Mar 1 [cited 2018 Aug 14];5(1):54–67. Available from: http://stacks.iop.org/1741-2552/5/i=1/a=006?key=crossref.c9d5638f9a5fad901b3b72c69ac1b84a

39. Datta A, Elwassif M, Battaglia F, Bikson M. Transcranial current stimulation focality using disc and ring electrode configurations: FEM analysis. J Neural Eng [Internet]. 2008 Jun 15 [cited 2018 Nov 2];5(2):163–74. Available from: http://stacks.iop.org/1741-2552/5/i=2/a=007?key=crossref.738fde56e272e2d6486eed0beaca23e7

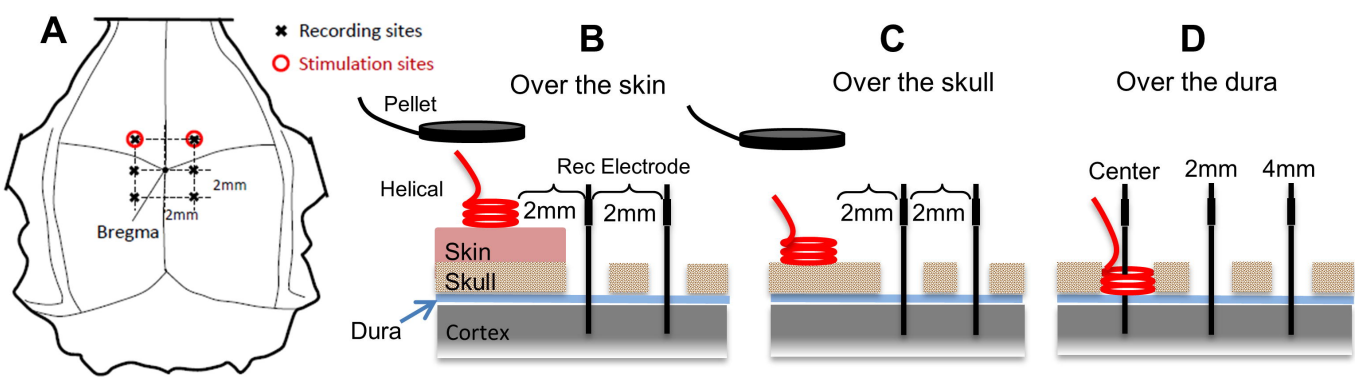
A
Recording sites
Stimulation sites
2mm
2mm
Bregma
B
Over the skin
Pellet
Helical
Rec Electrode
2mm
2mm
Skin
Skull
Dura
Cortex
C
Over the skull
2mm
2mm
D
Over the dura
Center
2mm
4mm

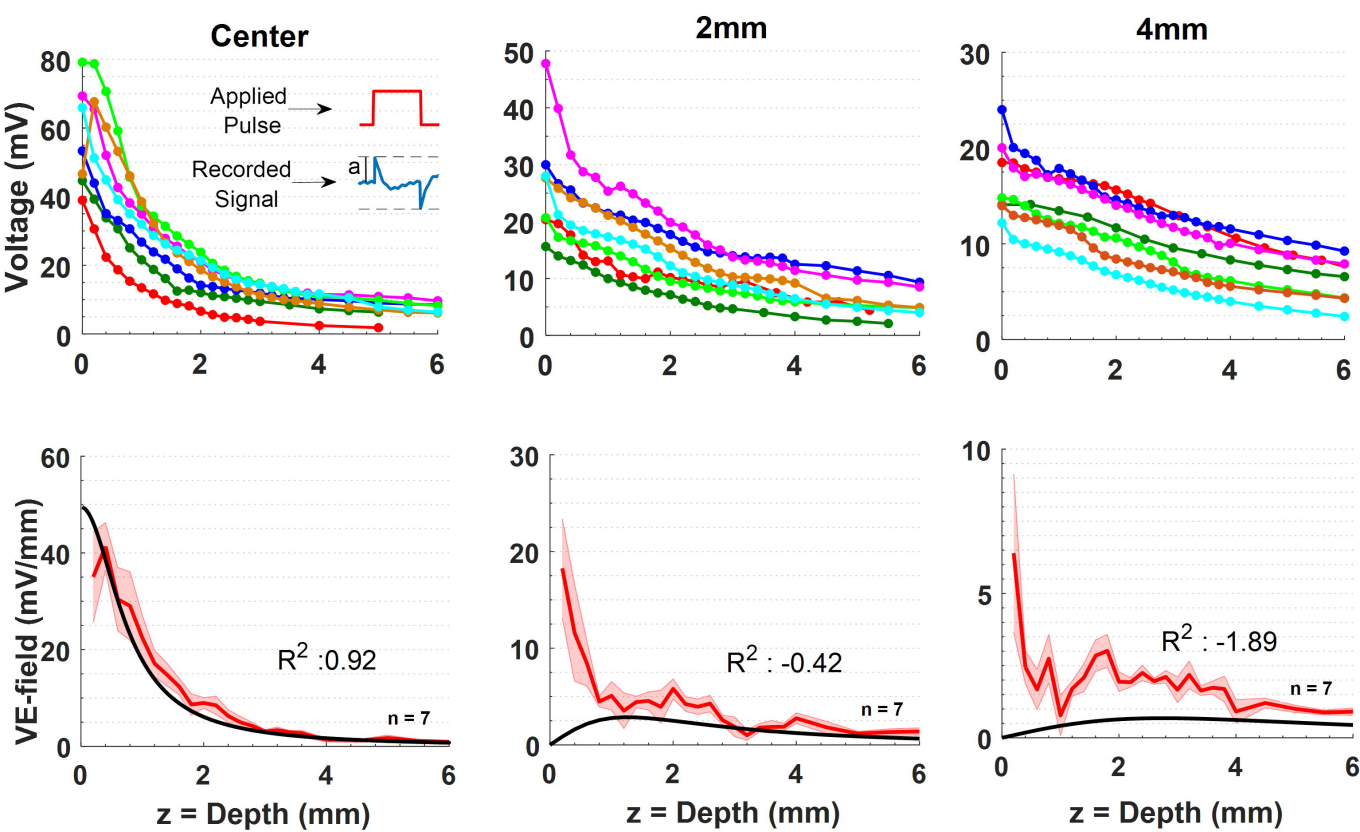
Center
2mm
4mm
Voltage (mV)
Applied Pulse
Recorded Signal
a
VE-field (mV/mm)
R^2 :0.92
R^2 : -0.42
R^2 : -1.89
n = 7
n = 7
n = 7
z = Depth (mm)
z = Depth (mm)
z = Depth (mm)

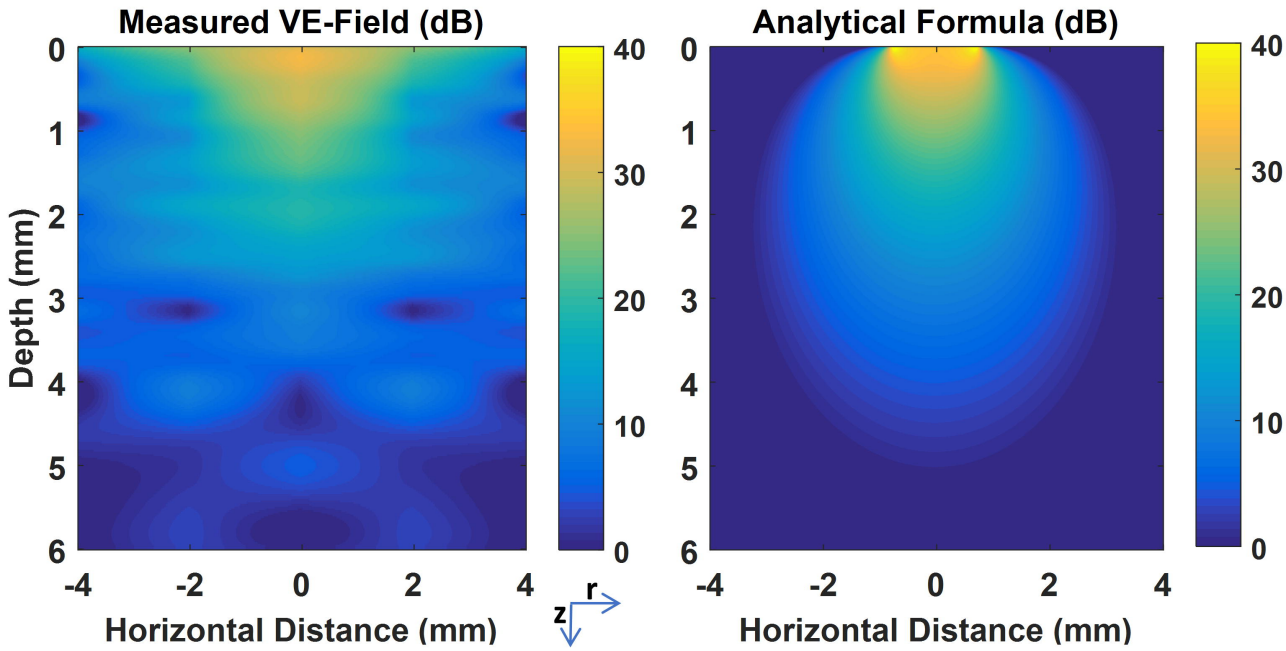
Measured VE-Field (dB)
Analytical Formula (dB)
Depth (mm)
0
1
2
3
4
5
6
-4
-2
0
2
4
Horizontal Distance (mm)
40
30
20
10
0
r
z

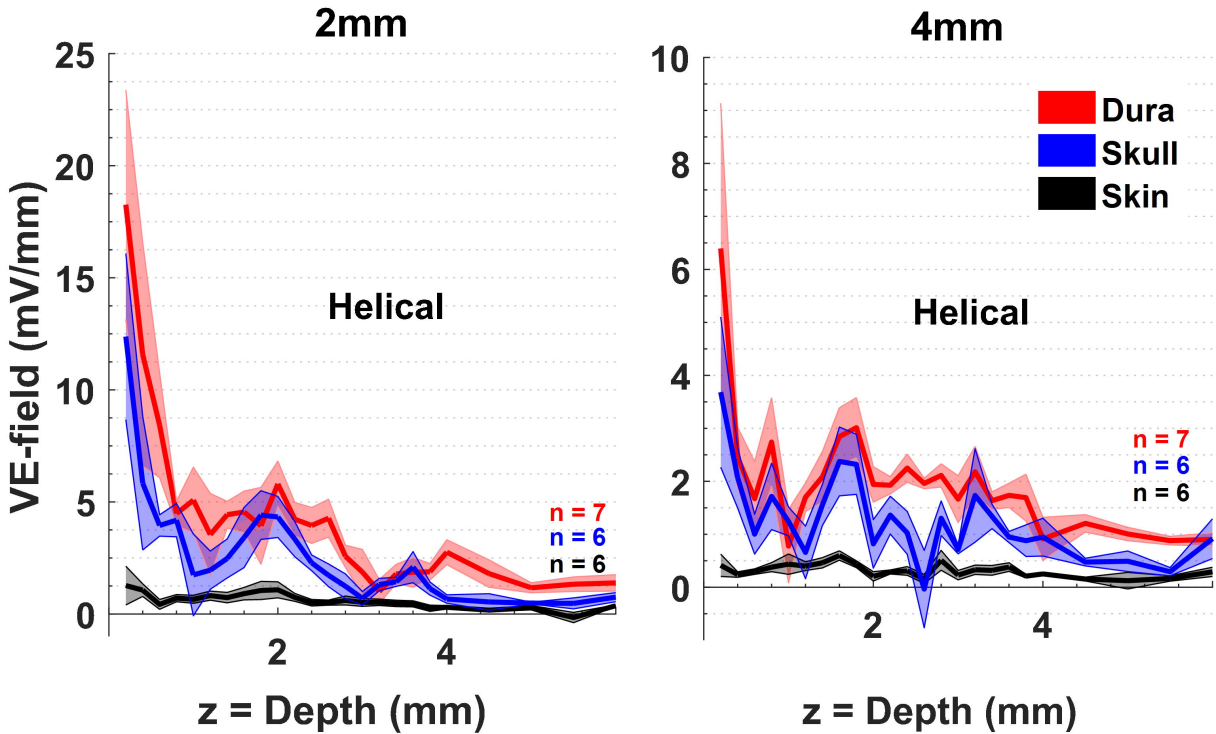
2mm
4mm
VE-field (mV/mm)
25
20
15
10
5
0
10
8
6
4
2
0
Helical
Helical
Dura
Skull
Skin
n = 7
n = 6
n = 6
n = 7
n = 6
n = 6
2
4
2
4
z = Depth (mm)
z = Depth (mm)

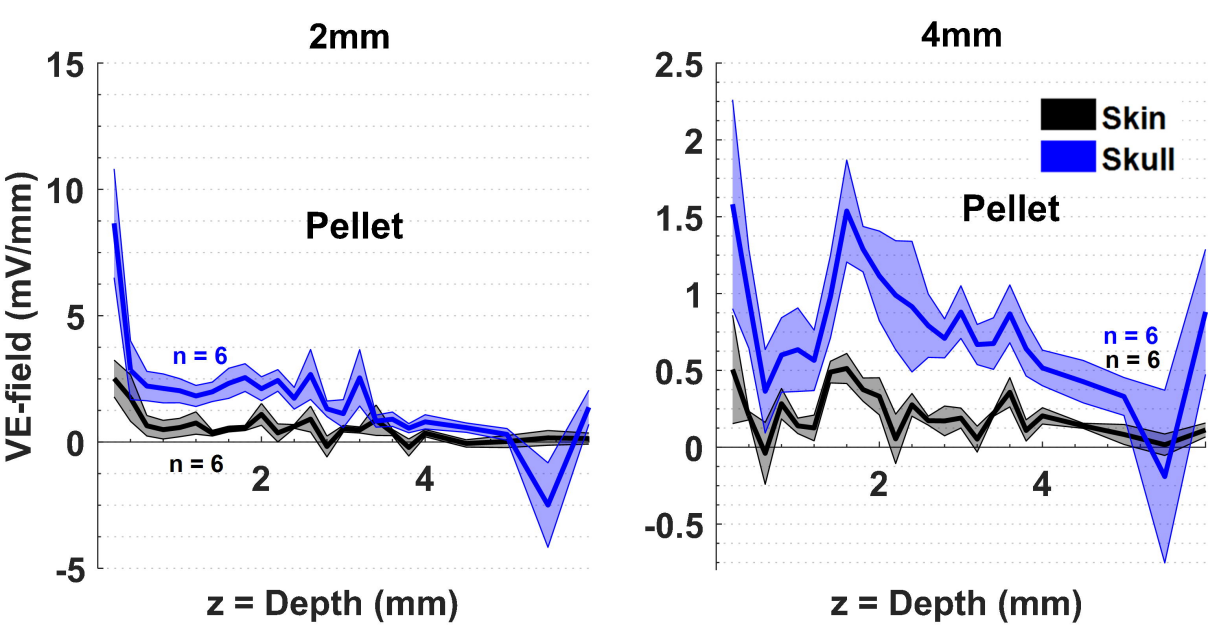
2mm
4mm
Pellet
Pellet
Skin
Skull
n = 6
n = 6
n = 6
n = 6
VE-field (mV/mm)
15
10
5
0
-5
2.5
2
1.5
1
0.5
0
-0.5
2
4
2
4
z = Depth (mm)
z = Depth (mm)